Nanoscale

Accepted Manuscript

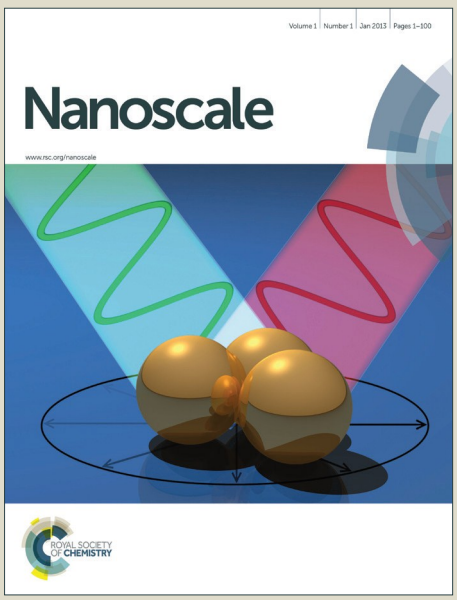

ROYAL SOCIETY OF CHEMISTRY

www.rsc.org/nanoscale

Nanoscale

RSCPublishing

COMMUNICATION

Co-assembly of Photosystem II/Reduced Graphene Oxide Multilayered Biohybrid Films for Enhanced Photocurrent

Cite this: DOI: 10.1039/x0xx00000x

Received 00th January 2012,
Accepted 00th January 2012

DOI: 10.1039/x0xx00000x

www.rsc.org/

Peng Cai,[a] Xiyun Feng,[a] Jinbo Fei,[a] Guangle Li,[a] Jiao Li[a,b], Huang Jianguo[b] and Junbai Li*[a]

A new type of biohybrid photo-electrochemical cell was fabricated by the layer-by-layer assembly of photosystem II and reduced graphene oxide. We demonstrate the photocurrent of the direct electron transfer is enhanced about two fold and with improved stability. The assembly strategy without any cross-linker or additional electron mediators permits the cell fabrication and operation much simpler as compared to previous approaches. This work may open new routes for the construction of solar energy conversion systems based on photoactive proteins and graphene materials.

Along with a demand for clean and renewable energy resources, the construction of highly-efficient and stable solar-energy conversion systems has become an important topic in current research.[1-3] Using artificial semiconductors as light absorbers has been the most popular approach.[4-6] Also, solar-to-fuel devices based on native photosystems promise great potential due to their low cost, environmental friendliness and high quantum yield.[7-10]

Photosystem II (PSII), found in thylakoid membranes of higher plants, algae and cyanobacteria, is the only protein known that can catalyze the light-driven water oxidation reaction.[11-13] Upon light absorption, it converts solar energy into chemical energy in concert with PSI, cytochrome b_6f, ATP synthase and other pigment-protein complexes. This concerted action provides the key challenge in mimicking the biological system. The oxidized primary electron donor, $P680^+$, reaches a reduction potential at about 1.25 V vs normal hydrogen electrode (NHE), which is high enough to oxidize water in a pH neutral aqueous solution. The maximum thermodynamic efficiency of this light energy to electrochemical potential conversion is about 70% for the optimum absorption wavelength.[7] These remarkable photocatalytic properties make it a promising building block in optoelectronic devices. Recently, extensive research efforts were directed towards the immobilization of PSII onto electrodes and the construction of photo-bioelectrochemical cells.[11,14,15] Different strategies and various materials have been used for engineering of these devices. For instance, PSII with a His-tag modified CP43 subunit was linked to a Ni-NTA-functionalized gold electrode.[16] By increasing the surface roughness of the electrode, the amount of immobilized PSII was increased and so the photocurrent was enhanced. Kato et al. reported a covalent way to tether PSII to the phosphonate modified electrode surface and further to improve direct electron transfer (DET) and stability of the proteins.[17] Unfortunately, many vital challenges remain since the quantum efficiency of isolated PSII cannot yet match the performance of *in vivo* PSII. Furthermore, present methods of PSII modification and immobilization require many steps. The introduction of additional high cost or hazardous electron mediators,[18,19] such as ruthenium complexes and methylene blue, makes the design and operation of the electrochemical cells more complicated.

Graphene-based materials are of great interest due to their extraordinary properties, such as large specific surface area, high electrical conductivity and excellent electrochemical stability.[20-24] The solution processing compatibility of reduced graphene oxide (rGO) makes the material more attractive for large area applications although lattice defects degrade its electrical properties. Among the enormous efforts devoted to the construction of graphene-based optoelectronic devices, rGO was mostly used as a 2D sheet to anchor semiconductor materials.[25,26] However, how graphene interacts with photoactive proteins and its potential in photo-bioelectrochemical cells has been rarely explored.

Herein, we construct a biohybrid photoanode with enhanced photocatalysis by integrating PSII enriched membranes with modified rGO *via* a very convenient and controllable layer-by-layer (LbL) assembly technique driven by electrostatic interaction (Figure 1a). The photocurrent generation diagram of the hybrid films above could be represented in Figure 1b. Upon light excitation, P680 is oxidized to produce a charge separation, which gives P680* (-0.58 V

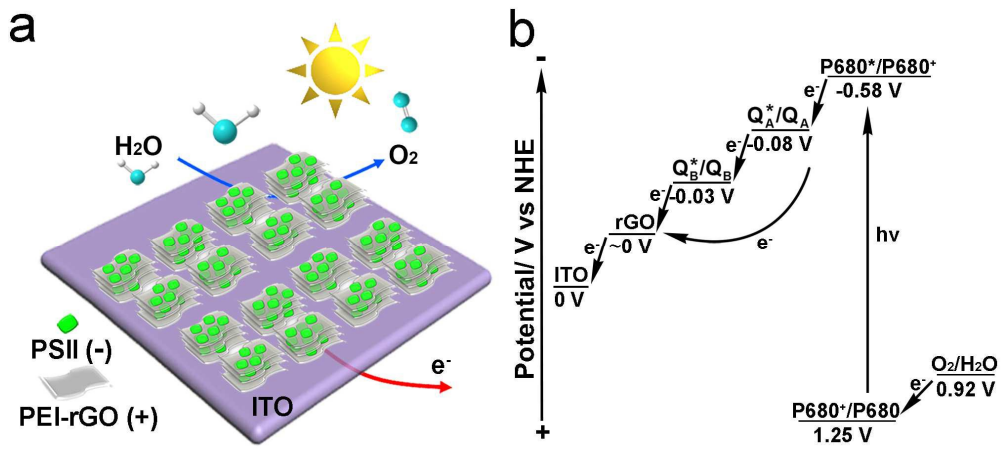

Figure 1. (a) Schematic representation of an ITO electrode functionalized with LbL co-assembly of negatively-charged PSII and positively-charged PEI-rGO multilayered films as a photoanode. (b) Schematic illustration for the relevant energy diagram.

vs NHE) and $P680^+$ (1.25 V vs NHE). $P680^+$ is reduced by extracting electrons from water (0.92 V vs NHE) in the electrolyte solution, generating a photocurrent and molecular oxygen. Meanwhile, the electrons from P680* are transferred to plastoquinones Q_A (-0.08 V vs NHE) and Q_B (-0.03 V vs NHE) *via* pheophytin.[7,27] The rGO sheets (~0 V vs NHE)[28] in the composite films can capture electrons from both Q_A and Q_B and readily transfer them to the indium tin oxide (ITO) substrates (0 V vs NHE).

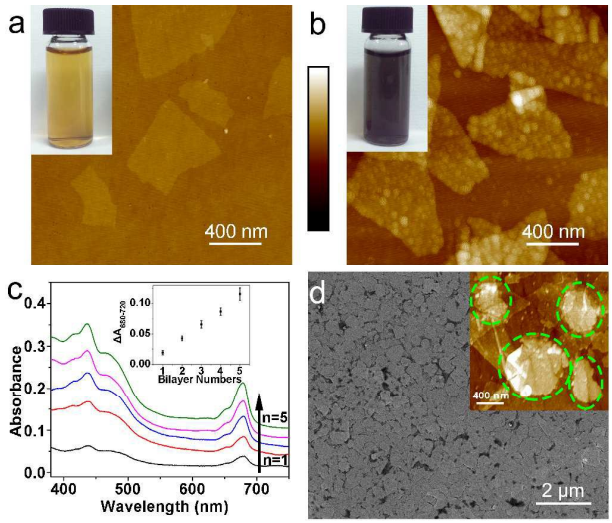

Figure 2. AFM images of (a) GO and (b) PEI-rGO on silicon wafers. Insets show the corresponding photographs of the GO and rGO aqueous dispersions. (c) UV-vis spectra of PEI-rGO/PSII multilayered films with varying numbers of LbL depositions on ITO substrate. Inset shows absorbance difference at 680 and 720 nm of PEI-rGO/PSII films on ITO substrate. (d) SEM image of $(PEI\text{-}rGO/PSII)_2$ films on ITO substrate. The inset is an AFM image of the $(PEI\text{-}rGO/PSII)_2$ films on ITO substrate. PSII enriched membranes are circled by green dashed lines. Z-scale bar is 30 nm for (a) and (b), 40 nm for inset of (d).

In a typical experiment, GO was synthesized from natural graphite using a modified Hummers method.[29] When GO was reduced by hydrazine, it was stabilized with polyethyleneimine (PEI) to form positively-charged PEI-rGO.[30] As shown in atomic force microscopy (AFM) image (Figure 2a), the average thickness of GO sheets is about 1.1 nm, which is in good agreement with previous reports.[25,26] After reduction and modification, densely packed PEI is clearly observed across the surface of the sheets with a thickness of 3.1 nm (Figure 2b), compared to the smooth and flat surface of GO sheets. The color of GO and PEI-rGO aqueous dispersions changed from light brown to dark grey, which indicates the reduction of GO (see Insets of Figure 2a and 2b). More details and relevant characterization are shown in the Supporting Information (Section I, Figure S1-S3). PSII enriched membranes were isolated and purified from spinach chloroplasts according to the methods introduced by Hankamer and Carpentier[31,32] (see Section II in Supporting Information). The results of sodium dodecyl sulfate polyacrylamide gel electrophoresis (SDS-PAGE), the UV-vis spectrum, and the AFM image show good agreement with those reported previously[33,34] (see Figure S4, S5 and S6, respectively). PEI-rGO nanosheets are positively charged (+29.2 mV) and PSII enriched membranes are negatively charged (-14.8 mV), implying that they can be co-assembled by electrostatic interaction. As expected, it can be seen from Figure 2c that with each deposition cycle of the PEI-rGO/PSII bilayer the light absorbance increased gradually. The same behavior can be found in the case of PEI/PSII multilayer films (Figure S7a). In particular, for PEI/PSII and PEI-rGO/PSII multilayered films, the relative amount of PSII absorbed was quantified by calculating the absorbance difference ($\Delta A_{680\text{-}720}$) at 680 and 720 nm considering the absorption background. In detail, the inset of Figure 2c shows that the amount of PSII absorbed increased linearly as a function of assembly cycle. This strongly signifies uniform and cumulative assembly of PSII in PEI-rGO/PSII films driven by electrostatic interaction. Also, the similar results can be found in PEI/PSII films (Figure S7b). Moreover, one can see that the surface coverage of PEI-rGO/PSII multilayered films increases when the number of bilayers increases (Figure S8, S9 and S10). In addition, it takes about 3 bilayers to cover the entire surface of the electrode substrate. For $(PEI\text{-}rGO/PSII)_2$, the scanning electron microscopy (SEM) and AFM images (Figure 2d and the inset) show that PEI-rGO sheets cover the electrode with PSII enriched membranes stacking on the surface.

In order to evaluate the photocurrent production of these biohybrid electrodes, photochronoamperometic measurements were

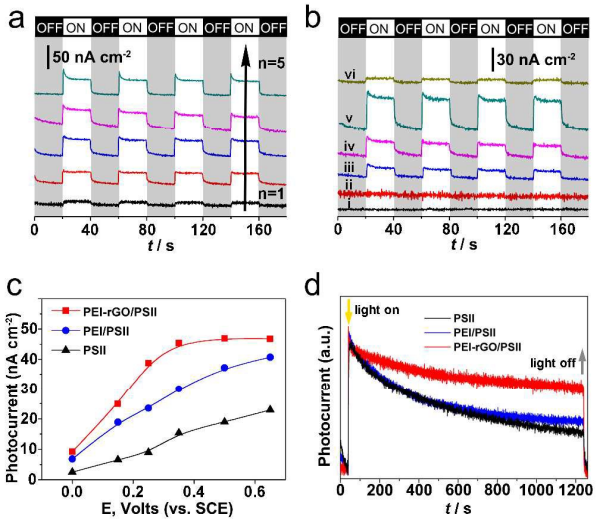

Figure 3. (a) Photocurrent response upon cyclically switched illumination of PEI-rGO/PSII multilayered films supported by ITO substrate. (b) Comparison of photocurrent response of (i) pure ITO, (ii) ITO-rGO, (iii) ITO-PSII, (iv) ITO-PEI/PSII (v) ITO-PEI-rGO/PSII and (vi) ITO-PEI-rGO/PSII with additional 30 μM 3-(3,4-dichlorophenyl)-1,1-dimethylurea (DCMU) as the inhibitor of PSII in electrolyte buffer solution. The later four films possesses the identical amount of PSII. (c) Dependence of the photocurrent on the external potential applied on ITO-PSII, ITO-PEI/PSII and ITO-PEI-rGO/PSII, respectively. d) Photocurrent stability of different electrodes under continuous light irradiation. The above photocurrents were measured with a bias potential of 0.25 V vs saturated calomel electrode (SCE) in an aqueous electrolyte buffer solution (pH 6.5, 20 mM 4-morpholinoethanesulfonic acid (MES), 50 mM KCl, 5 mM $MgCl_2$ and 3 mM $CaCl_2$) under light illumination (800 nm > λ > 550 nm, P_{680nm}=10 mW cm^{-2}) at 25 °C.

carried out. Figure S11 reveals that photocurrent action spectrum exhibits a peak at 680 nm. As shown in Figure 3a and Figure S12, the photocurrents of the ITO-(PEI-rGO/PSII)n increased gradually with the number of bilayers. Notably, increasing the amount of PSII could not lead to enhancement of photocurrent for the ITO-PSII films (data not shown). It means that the LbL assembly technique driven by electrostatic interaction has an advantage over pure physical deposition. In order to investigate the effect of rGO introduction on the photoelectrochemical performance of electrodes, we compared the photocurrents of different kinds of anodes possessing the similar amount of PSII. As Figure 3b shows, compared to ITO-PSII and ITO-PEI/PSII films, ITO-PEI-rGO/PSII exhibits much higher photocurrents. In detail, at a constant anode potential of 0.25 V, the DET photocurrent of ITO-PEI-rGO/PSII is 37.2 nA cm^{-2}, while it is only 9.2 and 19.9 nA cm^{-2} for ITO-PSII and ITO-PEI/PSII, respectively. That is, after statistical analysis (see Figure S13), in three anodes, the generated photocurrents per μg chlorophyll *a* are about 161.2, 39.1 and 81.7 nA, respectively. This could be attributed to the intimate contact between PSII and electrodes and the high electron transportation efficiency of graphene.[35] The influence of applied bias potential on the resulting photocurrent is displayed in Figure 3c. The photocurrent of ITO-PEI-rGO/PSII is always higher than those of other two anodes upon the same bias potentials. Additionally, it should be mentioned that the photocurrent of both multilayered films reaches a maximum at three bilayers (Figure S14). With the increase of deposition cycle, no further enhancement of the photocurrent was observed, which probably is due to an increasing resistance between the PSII and the electrode[36] and/or long electron transfer distances. The quantum efficiency of ITO-PEI-rGO/PSII is determined to be ~0.0026% and the value for ITO-PEI/PSII is about 0.0017%. It shows that the introduction of modified rGO indeed increases the quantum efficiency.

Light-induced decrease of photosynthetic activity, generally known as photoinhibition, is a general phenomenon in all photosynthetic organisms, especially in PSII.[37] In view of this point, the photocurrent stability of different films under continuous light irradiation was also investigated. As shown in Figure 3d, it can be seen that the stability of the films decreased as PEI-rGO/PSII>PEI/PSII>PSII. In detail, the PEI-rGO/PSII films remains about 65% of the initial photocurrent after illumination for 20 min, while ~40% and ~35% remains in PEI/PSII and PSII films. This can be attributed to a fast electron transfer process between PSII and PEI-rGO which reduces the photoinhibition of PSII caused by the formation of reactive oxygen species or damage of the manganese clusters.[15] Taken together, rGO sheets serve as an excellent electron acceptor and mediator in the hybrid films. Thus, photogenerated electrons from PSII can be transferred to the rGO sheets quickly through the delocalized π electrons, leading to enhanced photocurrent and reduced photo damage of PSII. Furthermore, comparing to other similar systems, this system has a comparatively low energy efficiency, but with a higher stability (shown in Table S1).

Conclusions

In summary, we have demonstrated a facile LbL assembly approach for the construction of ITO-PEI-rGO/PSII as photoelectrochemical cells. The obvious electrostatic interaction between the positively charged PEI-rGO and negatively charged PSII facilitates the electron transfer. PEI-rGO sheets act as both electron acceptor and mediator that electrically wire the photosystems with the electrodes. The co-assembled photoanode with improved stability and about two-fold enhancement of DET photocurrent confirms that rGO is a promising candidate for the integration with photoactive proteins. Higher photocurrent could be achieved by means of appropriate functionalization of graphene and optimized assembly process. This work thus provides a new strategy for the development of solar energy conversion systems based on photoactive proteins and graphene materials.

Acknowledgement

This work was supported financially by the National Natural Science Foundation of China (Project No. 21433010, 21320102004, 21321063) and National Basic Research Program of China (973 program, 2013CB932800, 2013YQ160551). We also wish to thank Prof. Michael Grunze for critically reading the manuscript.

Notes and references

[a] Beijing National Laboratory for Molecular Sciences (BNLMS), CAS Key Lab of Colloid, Interface and Chemical Thermodynamics, Institute of Chemistry, Chinese Academy of Sciences, Beijing 100190, China.
E-mail: jbli@iccas.ac.cn.
[b] Department of Chemistry, Zhejiang University, Hangzhou, Zhejiang 310027, China.

† Electronic supplementary information (ESI) available: Detailed experimental procedures, XRD patterns, UV-vis spectra, XPS spectra, SDS-PAGE patterns, AFM images and SEM images. See DOI: 10.1039/c000000x/

1 M. Grätzel, *Nature*, 2001, **414**, 338-344.
2 P. V. Kamat, *J. Phys. Chem. C*, 2007, **111**, 2834-2860.
3 M. G. Walter, E. L. Warren, J. R. McKone, S. W. Boettcher, Q. Mi, E. A. Santori and N. S. Lewis, *Chem. Rev.*, 2010, **110**, 6446-6473.
4 M. R. Hoffmann, S. T. Martin, W. Choi and D. W. Bahnemann, *Chem. Rev.*, 1995, **95**, 69-96.
5 M. Grätzel, *J. Photochem. Photobiol. C,* 2003, **4**, 145-153.
6 M. Ni, M. K. H. Leung, D. Y. C. Leung and K. Sumathy, Renew. Sust. *Energ. Rev.,* 2007, **11**, 401-425.
7 J. Barber, *Chem. Soc. Rev.*, 2009, **38**, 185-196.
8 T. Kothe, N. Plumere, A. Badura, M. M. Nowaczyk, D. A. Guschin, M. Rogner and W. Schuhmann, *Angew. Chem. Int. Ed. Engl.*, 2013, **52**, 14233-14236.
9 O. Yehezkeli, R. Tel-Vered, J. Wasserman, A. Trifonov, D. Michaeli, R. Nechushtai and I. Willner, *Nat. Commun*., 2012, **3**, 742.
10 K. S. Joya, Y. F. Joya, K. Ocakoglu and R. van de Krol, *Angew. Chem. Int. Ed. Engl.*, 2013, **52**, 10426-10437.
11 M. Kato, J. Z. Zhang, N. Paul and E. Reisner, *Chem. Soc. Rev.*, 2014.
12 K. Saito, A. W. Rutherford and H. Ishikita, *Proc. Natl. Acad. Sci. USA*, 2013, **110**, 954-959.
13 T. J. Meyer, M. H. Huynh and H. H. Thorp, *Angew. Chem. Int. Ed. Engl.*, 2007, **46**, 5284-5304.
14 O. Yehezkeli, R. Tel-Vered, D. Michaeli, I. Willner and R. Nechushtai, *Photosynth. Res.*, 2014, **120**, 71-85.
15 A. Badura, D. Guschin, B. Esper, T. Kothe, S. Neugebauer, W. Schuhmann and M. Rögner, *Electroanalysis*, 2008, **20**, 1043-1047.
16 N. Terasaki, M. Iwai, N. Yamamoto, T. Hiraga, S. Yamada and Y. Inoue, *Thin Solid Films*, 2008, **516**, 2553-2557.
17 M. Kato, T. Cardona, A. W. Rutherford and E. Reisner, *J. Am. Chem. Soc.*, 2013, **135**, 10610-10613.
18 B. A. Andersson, *Prog. Photovolt. Res. Appl.*, 2000, **8**, 61-76.
19 H.-W. Liang, X. Cao, W.-J. Zhang, H.-T. Lin, F. Zhou, L.-F. Chen and S.-H. Yu, *Adv. Funct. Mater.*, 2011, **21**, 3851-3858.
20 A. K. Geim and K. S. Novoselov, *Nat. Mater.*, 2007, **6**, 183-191.
21 S. Stankovich, D. A. Dikin, G. H. B. Dommett, K. M. Kohlhaas, E. J. Zimney, E. A. Stach, R. D. Piner, S. T. Nguyen and R. S. Ruoff, *Nature*, 2006, **442**, 282-286.
22 C. Li and G. Shi, *Nanoscale*, 2012, **4**, 5549-5563.
23 R. R. Nair, P. Blake, A. N. Grigorenko, K. S. Novoselov, T. J. Booth, T. Stauber, N. M. R. Peres and A. K. Geim, *Science*, 2008, **320**, 1308.
24 C. Lee, X. Wei, J. W. Kysar and J. Hone, *Science*, 2008, **321**, 385-388.
25 F. X. Xiao, J. Miao and B. Liu, *J. Am. Chem. Soc.*, 2014, **136**, 1559-1569.
26 H. Hayashi, I. V. Lightcap, M. Tsujimoto, M. Takano, T. Umeyama, P. V. Kamat and H. Imahori, *J. Am. Chem. Soc.*, 2011, **133**, 7684-7687.
27 J. P. McEvoy and G. W. Brudvig, *Chem. Rev.*, 2006, **106**, 4455-4483.
28 R. Czerw, B. Foley, D. Tekleab, A. Rubio, P. Ajayan and D. Carroll, *Phys. Rev. B*, 2002, **66**.
29 W. S. Hummers and R. E. Offeman, *J. Am. Chem. Soc.*, 1958, **80**, 1339-1339.
30 L. Dai, *Acc. Chem. Res.*, 2012, **46**, 31-42.
31 B. Hankamer, J. Nield, D. Zheleva, E. Boekema, S. Jansson and J. Barber, *Eur. J. Biochem.*, 1997, **243**, 422-429.
32 Y. Yamamoto, J. Leng and J.-R. Shen, in *Photosynthesis Research Protocols*, ed. R. Carpentier, Humana Press, 2011, pp. 1-10.
33 H. Kirchhoff, S. Lenhert, C. Büchel, L. Chi and J. Nield, *Biochemistry*, 2008, **47**, 431-440.
34 W. Wang, J. Chen, C. Li and W. Tian, *Nat. Commun.*, 2014, **5**, 4647.
35 E. Darby, G. LeBlanc, E. A. Gizzie, K. M. Winter, G. K. Jennings and D. E. Cliffel, *Langmuir*, 2014, **30**, 8990-8994.
36 O. Yehezkeli, R. Tel-Vered, D. Michaeli, R. Nechushtai and I. Willner, *Small*, 2013, **9**, 2970-2978.
37 E.-M. Aro, I. Virgin and B. Andersson, Biochim. Biophys. Acta, 1993, **1143**, 113-134.